



Open
Access

Influence of Variable Transport Properties on Casson Nanofluid Flow over a Slender Riga Plate: Keller Box Scheme

Kerehalli Vinayaka Prasad¹, Hanumesh Vaidya^{1,*}, Gudekote Manjunatha², Kuppalapalle Vajravelu³, Choudhari Rajashekhar², V. Ramanjini¹

¹ Department of Mathematics, VSK University, Vinayaka Nagar, Ballari-583 105, Karnataka, India

² Department of Mathematics, Manipal Institute of Technology, Manipal Academy of Higher Education, Manipal, Karnataka, India

³ Department of Mathematics, University of Central Florida, Orlando, FL 32816, USA

ARTICLE INFO

ABSTRACT

Article history:

Received 12 July 2019

Received in revised form 25 September 2019

Accepted 26 September 2019

Available online 15 December 2019

In this article, an analysis has been carried out to study the effects of variable viscosity and variable thermal conductivity on the heat transfer characteristics of a Casson nanofluid over a slender Riga plate with zero mass flux and melting heat transfer boundary conditions. The nonlinear governing equations with the suitable boundary conditions are initially cast into dimensionless form by similarity transformations. The resulting coupled highly nonlinear equations are solved numerically by an efficient second-order finite difference scheme known as Keller Box Method. The effect of various physical parameters on velocity, temperature, and concentration profiles are illustrated through graphs and the numerical values are presented in tables. One of the critical findings of our study is that the effect of variable viscosity on velocity shows reducing nature, but there is an increasing nature in temperature and concentration.

Keywords:

Riga plate; Melting heat transfer; variable fluid properties; Keller box method

Copyright © 2019 PENERBIT AKADEMIA BARU - All rights reserved

1. Introduction

In recent years, controlling the flow of electrically conducting fluids is one of the primary tasks to the scientists and engineers. The controlled flow of these fluids has enormous applications in industrial and technological processes involving heat and mass transfer phenomenon. However, the polymer industry has adopted a few conventional methods to control the fluid flow such as of suction/blowing and wall motion methods with the assistance of electromagnetic body forces. The flow of the fluids having high electrical conductivity such as liquid metals, plasma, and electrolytes, etc. can be significantly controlled by applying an external magnetic field. This concept can be used for controlling the classical electro magnetohydrodynamic (EMHD) fluid flows. In view of the industrial applications, Gailitis, and Lielausis [1] of the physics institute in Riga, the capital city of the Latvia country designed one of the devices known as Riga plate to generate simultaneous electric

* Corresponding author.

E-mail address: hanumeshvaidya@gmail.com (Hanumesh Vaidya)

and magnetic fields which can produce Lorentz force parallel to the wall in weakly conducting fluids. This plate consists of a spanwise aligned array of alternating electrodes and permanent magnets mounted on a plane surface. This array generates a surface-parallel Lorentz force with a neglected pressure gradient, which decreases exponentially in the direction normal to the (horizontal) plate. However, in vector product form the volume density of a Lorentz force is written as $\mathbf{F}_1 = \mathbf{J} \times \mathbf{B}$ and in terms of Ohm's law it can be expressed as $\mathbf{J} = \sigma(\mathbf{E} + \mathbf{V} \times \mathbf{B})$ where σ is an electrical conductivity of the fluid, \mathbf{V} is the fluid velocity, and \mathbf{E} is the electric field. In the absence of any extrinsic magnetic field, a complete contactless flow can be attained when $\sigma \approx 10^{-6}$ S/m. Where as in the presence of extrinsic magnetic field, an induced high current density $\sigma(\mathbf{V} \times \mathbf{B})$ can be obtained and we have $\mathbf{F}_1 = \mathbf{J} \times \mathbf{B} = \sigma(\mathbf{V} \times \mathbf{B}) \times \mathbf{B} = \sigma[(\mathbf{V} \times \mathbf{B})\mathbf{B} - \mathbf{B}^2\mathbf{V}]$. On the contrary, when $\sigma \approx 10^6$ S/m, a low current density $\sigma(\mathbf{V} \times \mathbf{B})$ can be seen. To tackle with such cases, an extrinsic magnetic field is used to obtain the EMHD flow. The expression $\mathbf{F}_1 = \mathbf{J} \times \mathbf{B} \approx \sigma(\mathbf{E} \times \mathbf{B})$ reveals that the electrical conductivity of a fluid is very small, and it does not rely upon the flow field. According to Grinberg [2], the density force can be written as $\mathbf{F}_1 = \frac{\pi_1 M_0 j_0}{8} e^{-\frac{\pi_1 y}{a}}$. Tsinober and Shtern [3]

observed the substantial improvement in the strength of the Blasius flow towards a Riga plate, which is due to the more significant influence of wall parallel Lorentz forces. Further, the boundary layer flow of low electrical conductivity of fluids over a Riga plate was scrutinized by Pantokratoras and Magyari [4]. Pantokratoras [5] extended the work of Pantokratoras and Eugen [4] to Blasius and Sakiadis flow.

In addition to controlling the flow of electrically conducting fluids, the technological industry demands the control of heat transfer in a process. This can be achieved with the help of nanofluids technology. Nanofluid is the blend of the nanometer-scale (1nm to 100 nm) solid particles and low thermal conductivity base liquids such as water, ethylene glycol (EG), oils, etc. Two different phases are used to simulate nanofluid. In both the methods researchers assumed as the common pure fluid and more precisely in the second method, the mixer or blend is with the variable concentration of nanoparticles. Choi [6] proposed the term nanofluid and verified that the thermal conductivity of fluids could be improved by the inclusion of nanometer-sized metals (Cu, Ag, Au), oxides (Al_2O_3 , CuO), carbide ceramics (SiC, TiC/carbon nanotubes/fullerene) into the base fluids. Buongiorno [7] established that Brownian diffusion and thermophoresis are important slip mechanisms in nanofluids. Makinde and Aziz [8] examined the impact of Brownian motion and thermophoresis on transport equations numerically. Ahmad *et al.*, [9] and Ayub *et al.*, [10] examined the boundary layer flow of nanofluid due to Riga plate. Further, Hayat *et al.*, [11, 12] analysed squeezing flow of a nanofluid between two parallel Riga plates by considering different external effects. Recently, Naveed *et al.*, [13] continued the work of Ref [12] and studied salient features of ($\text{Ag-Fe}_3\text{O}_4/\text{H}_2\text{O}$) hybrid nanofluid between two parallel Riga plates. Furthermore, several research articles can be found in the literature that covers the different physical and geometrical aspects of the classical liquids. Few of them can be seen in the references. [14-25].

All the researchers, as mentioned earlier, have concentrated on conventional nonlinear stretching but not on the stretching. Fang *et al.*, [26] have coined the word variable thickness for the specific type of nonlinear stretching and examined the performance of boundary layer flow over a stretching sheet with variable thickness. Khader and Megahed [27] reviewed the work of Fang *et al.*, [26] via Numerical method to explain velocity slip effects. Farooq *et al.*, [28] considered variable thickness geometry with Riga plate to analyze stagnation point flow and Prasad *et al.*, [29-

33] examined the impact of variable fluid properties on the Newtonian/non-Newtonian fluid flow field.

The main objective of the present work is to reduce the skin friction or drag force of the fluids by applying an external electric field in the presence of variable fluid properties over a slender elastic Riga plate under the influence of zero mass flux and heat transfer boundary conditions. Suitable similarity variables are introduced to transform the coupled nonlinear partial differential equations into a set of coupled nonlinear ordinary differential equations. These equations are solved numerically via Keller Box method (See Vajravelu and Prasad [34]). The effects of various governing physical parameters for velocity, temperature, and nanoparticle concentration are discussed through the graphs and tables. The obtained results are compared with the actual results in previous literature and are found to be in excellent agreement. From this, it can be concluded that the present research work provides useful information for Science and industrial sector.

2. Mathematical Analysis of the Problem

Consider an electromagnetic flow of a steady, incompressible non-Newtonian nanofluid over a slender Riga plate with variable fluid properties. Here the non-Newtonian fluid model is the Casson model and the rheological equation of state for an isotropic and incompressible fluid is given by (for details see, Prasad *et al.*, [32]).

$$\tau_{ij} = \begin{cases} 2(\mu_B + P_y / \sqrt{2\pi})e_{ij}, \pi > \pi_c \\ 2(\mu_B + p_y / \sqrt{2\pi_c})e_{ij}, \pi < \pi_c \end{cases} \quad (1)$$

where $\pi = e_{ij}e_{ij}$ and e_{ij} is the $(i, j)^{th}$ component of deformation rate, π is the product of the component of deformation rate with itself, π_B is the plastic dynamic viscosity of Casson fluid, P_y is yield stress of the fluid and π_c is a critical value of this product depending on the non-Newtonian model. Further, the Riga plate is considered as an alternating array consisting of electrodes and permanent magnets mounted on a plane surface situated at $y = 0$ having x-axis vertically upwards. The fluid is characterized by a nanoparticle and is analyzed by considering Brownian motion and thermophoresis phenomena. The following assumptions are made

- i. Joule heating and viscous dissipation are neglected.
- ii. The fluid is isotropic, homogeneous, and has constant electric conductivity.
- iii. The velocity of the stretching Riga plate and the free stream velocity are respectively, assumed to be $U_w(x) = U_0(x+b)^m$ and $U_e(x) = U_\infty(x+b)^m$, where U_∞ and U_0 are positive constants, m is the velocity power index and b is the physical parameter related to slender elastic sheet.
- iv. The Riga plate is not flat and is defined as $y = A(x+b)^{(1-m)/2}$, $m \neq 1$, where the coefficient A is chosen as small so that the sheet is sufficiently thin, to avoid pressure gradient along the Riga plate ($\partial p / \partial x = 0$)
- v. The temperature and nanoparticle concentration at the melting variable thickness of the Riga plate are T_M and C_M respectively and further T_∞ and C_∞ denote the ambient temperature and nanoparticle concentration of the fluid respectively.
- vi. For different applications, the thickness of the stretching Riga plate is assumed to vary with the distance from the slot due to acceleration/deceleration of an extruded plate.

For $m = 1$ thickness of the plate become flat. The physical model of the problem is given below (Figure 1).

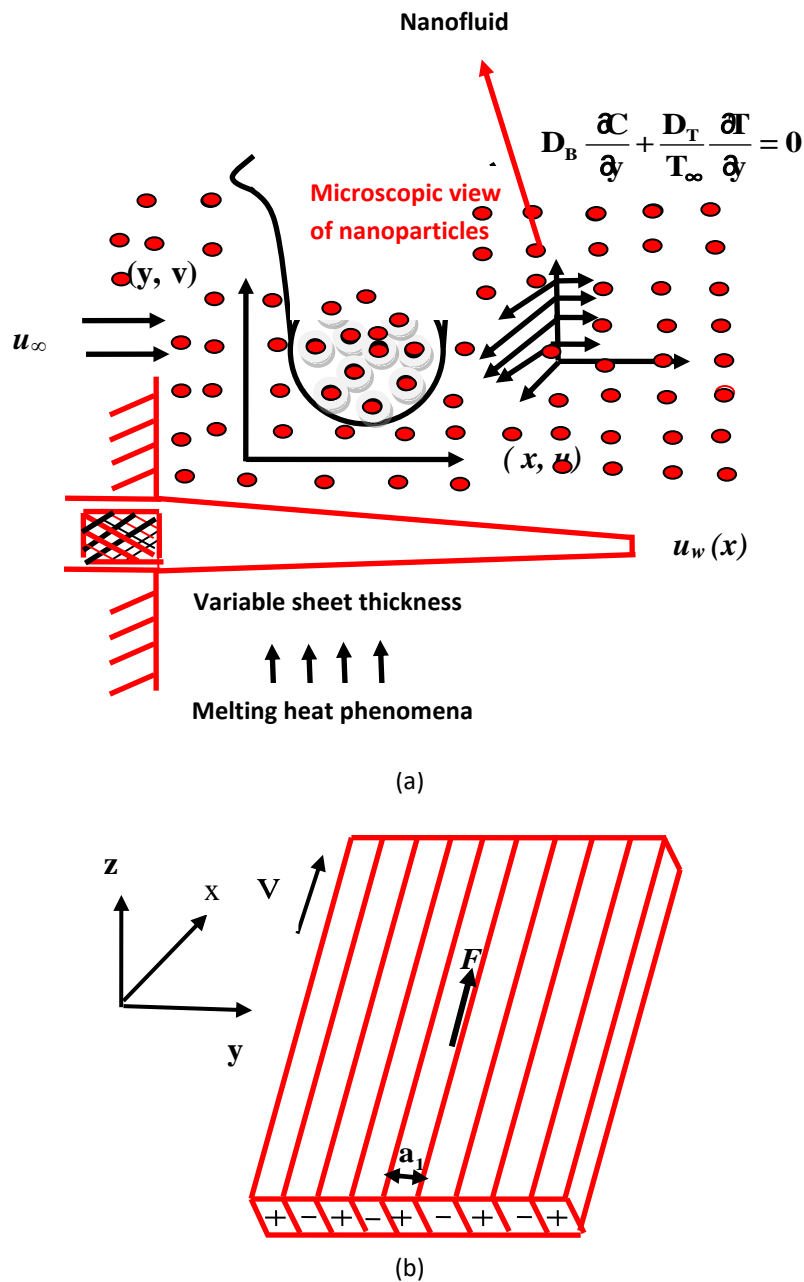


Fig. 1. Physical model of (a) variable thickness and (b) Riga plate

Based on the above assumptions and the usual boundary layer approximations, the governing equations for continuity, momentum, thermal energy, and concentration for the nanofluid model are expressed as follows

$$\frac{\partial u}{\partial x} + \frac{\partial v}{\partial y} = 0 \tag{2}$$

$$u \frac{\partial u}{\partial x} + v \frac{\partial u}{\partial y} = \left(1 + \frac{1}{\beta}\right) \frac{1}{\rho_\infty} \frac{\partial}{\partial y} \left(\mu(T) \frac{\partial u}{\partial y} \right) + U_e \frac{dU_e}{dx} + \frac{\pi_1 j_0 M_0(x)}{8\rho_\infty} \exp\left(\frac{-\pi_1}{a_1(x)} y\right) \quad (3)$$

$$u \frac{\partial T}{\partial x} + v \frac{\partial T}{\partial y} = \frac{1}{\rho_\infty c_p} \frac{\partial}{\partial y} \left(K(T) \frac{\partial T}{\partial y} \right) + \frac{Q_0(x)}{\rho_\infty c_p} (T - T_\infty) + \tau \left[D_B(C) \frac{\partial C}{\partial y} \frac{\partial T}{\partial y} + \frac{D_T}{T_\infty} \left(\frac{\partial T}{\partial y} \right)^2 \right] \quad (4)$$

$$u \frac{\partial C}{\partial x} + v \frac{\partial C}{\partial y} = \frac{\partial}{\partial y} \left(D_B(C) \frac{\partial C}{\partial y} \right) + \frac{D_T}{T_\infty} \frac{\partial^2 T}{\partial y^2} \quad (5)$$

where u and v are velocity components along x and y directions respectively. β is the Casson parameter, c_p is the specific heat at constant pressure, and ρ_∞ is the fluid density. The transport properties of the fluid are assumed to be constant, except for the fluid viscosity $\mu(T)$, the fluid thermal conductivity $K(T)$ and Brownian diffusion of the fluid D_B , are assumed to be functions of temperature and nanoparticle concentration, and are expressed as follows

$$\mu(T) = \mu_\infty [1 + \delta(T - T_M)]^{-1}, \text{ i.e. } \mu(T) = [a_2(T - T_r)]^{-1}, \quad (6)$$

$$K(T) = K_\infty [1 + \varepsilon_1((T - T_M)/(T_\infty - T_M))] \quad (7)$$

$$D_B(C) = D_{B_\infty} [1 + \varepsilon_2((C - C_M)/(C_\infty - C_M))] \quad (8)$$

here $a_2 = \delta / \mu_\infty$ and $T_r = T_\infty - 1/\delta$ are constants and their values depend on the reference state and the small parameter δ is known as thermal property of the fluid. Generally, the positive and negative values of a_2 describes two different states, namely, liquids and gases respectively, i.e. for $a_2 > 0$ represents the liquid state and $a_2 < 0$ represents gas state. Here μ_∞ , K_∞ and D_{B_∞} are ambient fluid viscosity, thermal conductivity and Brownian diffusion coefficient respectively. ε_1 and ε_2 are small parameters known as the variable thermal conductivity parameter and variable species diffusivity parameter respectively. The term $Q_0(x)$ represents the heat generation when $Q_0 > 0$ and heat absorption when $Q_0 < 0$, and are used to describe exothermic and endothermic chemical reactions respectively. Further, j_0 is the applied current density in the electrodes, $M_0(x)$ is the magnetization of the permanent magnets mounted on the surface of the Riga plate and $a_1(x)$ is width between the magnets and electrodes. The special forms $Q_0(x) = Q_0(x+b)^{(1-m)/2}$, $M_0(x) = M_0(x+b)^{(1-m)/2}$ and $a_1(x) = a_1(x+b)^{(1-m)/2}$ are chosen to obtain the similarity solutions. τ is defined as the ratio between the effective heat capacity of the nanoparticle material and heat capacity of the fluid, i.e. $\tau = (\rho_\infty c_p)_p / (\rho_\infty c_p)_f$, D_T is the thermophoresis diffusion coefficient and T_0 is solid temperature. The appropriate boundary conditions are

$$\left. \begin{aligned} u &= U_w(x) = U_0(x+b)^m, \\ K(\partial T/\partial y) &= \rho[\lambda_1 + c_s(T_M - T_0)]v(x,y), T = T_M \\ D_B \frac{\partial C}{\partial y} + \frac{D_T}{T_\infty} \frac{\partial T}{\partial y} &= 0 \end{aligned} \right\} \text{at } y = A(x+b)^{1-m/2} \quad (9)$$

$$u \rightarrow U_e(x) = U_\infty(x+b)^m, \quad T \rightarrow T_\infty, \quad C \rightarrow C_\infty \quad \text{as } y \rightarrow \infty$$

The second boundary condition defined in Eq. (9) $K(\partial T/\partial y) = \rho[\lambda_1 + c_s(T_M - T_0)]v(x,y)$ represents the melting temperature in which λ_1 is the latent heat of fluid, T_M is the melting temperature, T_0 and C_s are the temperature and heat capacity of the concrete surface respectively. On substituting Eq. (6)-(8) in the basic Eq. (3)-(5), it reduces to

$$u \frac{\partial u}{\partial x} + v \frac{\partial u}{\partial y} = \left(1 + \frac{1}{\beta}\right) \frac{1}{\rho_\infty} \frac{\partial}{\partial y} \left(\frac{\mu_\infty}{1 + \delta(T - T_\infty)} \frac{\partial u}{\partial y} \right) + U_e \frac{dU_e}{dx} + \frac{\pi j_0 M_0(x)}{8\rho_\infty} \exp\left(\frac{-\pi}{a_1(x)} y\right) \quad (10)$$

$$u \frac{\partial T}{\partial x} + v \frac{\partial T}{\partial y} = \frac{\partial}{\partial y} \left(\frac{K_\infty}{\rho_\infty c_p} \left(1 + \varepsilon_1 \left(\frac{T - T_M}{T_\infty - T_M}\right)\right) \frac{\partial T}{\partial y} \right) + \frac{Q_0(x)}{\rho_\infty c_p} (T - T_\infty) + \tau \left[D_{B_\infty} \left(1 + \varepsilon_2 \left(\frac{C - C_M}{C_\infty - C_M}\right)\right) \frac{\partial C}{\partial y} \frac{\partial T}{\partial y} + \frac{D_T}{T_\infty} \left(\frac{\partial T}{\partial y}\right)^2 \right] \quad (11)$$

$$u \frac{\partial C}{\partial x} + v \frac{\partial C}{\partial y} = \frac{\partial}{\partial y} \left(D_{B_\infty} \left(1 + \varepsilon_2 \left(\frac{C - C_M}{C_\infty - C_M}\right)\right) \frac{\partial C}{\partial y} \right) + \frac{D_T}{T_\infty} \frac{\partial^2 T}{\partial y^2} \quad (12)$$

Now, we transform the system of Eq. (10)-(12) into dimensionless form. To this end, the dimensionless similarity variable be,

$$\eta = y \sqrt{(m+1/2) \frac{U_0(x+b)^{(m-1)}}{v_\infty}} \quad (13)$$

and the dimensionless stream function, the dimensionless temperature and the dimensionless nanoparticle concentration are,

$$\psi = \sqrt{(2/m+1)v_\infty U_0(x+b)^{(m+1)}} F(\eta), \quad \Theta(\eta) = \frac{T - T_M}{T_\infty - T_M}, \quad \Phi(\eta) = \frac{C - C_M}{C_\infty - C_M} \quad (14)$$

with the use of Eq. (13) and (14), the velocity components are,

$$u = \partial\psi/\partial y = U_0(x+b)^m F'(\eta), \quad v = -\partial\psi/\partial x = -\sqrt{\frac{2}{(m+1)} v_\infty U_0(x+b)^{(m-1)}} \left[\frac{(m+1)}{2} F(\eta) + \eta \frac{(m-1)}{2} F'(\eta) \right] \quad (15)$$

here prime denotes differentiation with respect to η . In the present work, it is assumed $m > -1$ for the validity of the similarity variable. With the use of Eq. (13)-(15), then Eq. (10)-(12) and the corresponding boundary conditions reduce to:

$$\left(1 + \frac{1}{\beta}\right) \left(\left(1 - \frac{\Theta}{\theta_r}\right)^{-1} F'' \right)' + FF'' - \frac{2m}{(m+1)} (F')^2 + \frac{2m}{(m+1)} A^* + \frac{2}{(m+1)} Qe^{-\beta_1\eta} = 0 \quad (16)$$

$$\left((1 + \varepsilon_1\Theta)\Theta' \right)' + \text{Pr}\Theta' [Nb(1 + \varepsilon_2\Phi)\Phi' + Nt\Theta' + F] + \frac{2}{(m+1)} \text{Pr}\lambda\Theta = 0 \quad (17)$$

$$\left((1 + \varepsilon_2\Phi)\Phi' + \left(\frac{Nt}{Nb}\right)\Theta' \right)' + LeF\Phi' = 0 \quad (18)$$

$$M\Theta'(\alpha) + \text{Pr} \left[F(\alpha) - \frac{\alpha(1-m)}{(1+m)} \right] = 0, \quad F'(\alpha) = 1, \quad \Theta(\alpha) \rightarrow 0, \quad (19)$$

$$Nb\Phi'(\alpha) + Nt\Theta'(\alpha) = 0, \quad F'(\infty) \rightarrow A^*, \quad \Theta(\infty) \rightarrow 1, \quad \Phi(\infty) \rightarrow 1$$

The non-dimensional parameters $\theta_r, A^*, Q, \beta_1, \text{Pr}, \alpha, Nb, Nt, \lambda, Le$ and M represent the variable viscosity parameter, stretching rate ratio parameter, modified Hartman number, dimensionless parameter, Prandtl number, wall thickness parameter, Brownian motion parameter, thermophoresis parameter, heat source/sink parameter, Lewis number and the dimensionless melting heat parameter respectively and which are defined as follows

$$\theta_r = \frac{-1}{\delta(T_\infty - T_M)}, \quad A^* = \frac{U_\infty}{U_0}, \quad Q = \frac{\pi j_0 M_0}{8\rho_\infty U_0^2}, \quad \beta_1 = \frac{\pi}{a_1} \sqrt{\frac{2}{(m+1)} \frac{v_\infty}{U_0(x+b)^{(m-1)}}}, \quad \text{Pr} = \frac{v_\infty}{\alpha_\infty}, \quad \alpha = A \sqrt{\frac{U_0(m+1)}{2v_\infty}}, \quad (20)$$

$$Nb = \frac{\tau_\infty D_{B_\infty} (C_\infty - C_M)}{v_\infty}, \quad Nt = \frac{\tau_\infty D_{T_\infty} (T_\infty - T_M)}{T_\infty v_\infty}, \quad \lambda = \frac{Q_0}{\rho_\infty c_p U_0}, \quad Le = \frac{v_\infty}{D_{B_\infty}} \quad \text{and} \quad M = \frac{c_p (T_\infty - T_M)}{\lambda_1 + c_s (T_M - T_0)}$$

The value of the θ_r is determined by the viscosity of the fluid under consideration, it is worth mentioning here that for $\delta \rightarrow 0$ i.e. $\mu = \mu_\infty$ (constant) then $\theta_r \rightarrow \infty$. It is also important to note that θ_r is negative for liquids and positive for gases when $(T_\infty - T_M)$ is positive, this is due to fact that the viscosity of a liquid usually decreases with increasing in temperature. Further, $M = 0$ shows that there is no melting phenomenon, also it should be noted that M comprises of the Stefan constants $c_p(T_\infty - T_0)/\lambda_1$ and $c_s(T_M - T_0)$ of liquid and solid phase respectively. Now, we define the following $F(\eta) = f(\eta - \alpha) = f(\xi), \Theta(\eta) = \theta(\eta - \alpha) = \theta(\xi), \Phi(\eta) = \phi(\eta - \alpha) = \phi(\xi)$, here $\eta = \alpha$ indicates the flat surface. Then Eq. (16) to (19) reduce to

$$\left(1 + \frac{1}{\beta}\right) \left(\left(1 - \frac{\theta}{\theta_r}\right)^{-1} f'' \right)' + ff'' - \frac{2m}{(m+1)} (f')^2 + \frac{2m}{(m+1)} A^* + \frac{2}{(m+1)} Qe^{-\beta_1(\xi+\alpha)} = 0 \quad (21)$$

$$\left((1 + \varepsilon_1 \theta) \theta' \right)' + \text{Pr} \theta' (Nb(1 + \varepsilon_2 \phi) \phi' + Nt \theta' + f) + \frac{2}{(m+1)} \text{Pr} \lambda \theta = 0 \quad (22)$$

$$\left((1 + \varepsilon_2 \phi) \phi' + \left(\frac{Nt}{Nb} \right) \theta' \right)' + Lef \phi' = 0 \quad (23)$$

$$M \theta'(0) + \text{Pr} \left[f(0) - \frac{\alpha(1-m)}{(1+m)} \right] = 0, \quad f'(0) = 1, \quad \theta(0) \rightarrow 0, \quad (24)$$

$$Nb \phi'(0) + Nt \theta'(0) = 0, \quad f'(\infty) \rightarrow A^*, \quad \theta(\infty) \rightarrow 1, \quad \phi(\infty) \rightarrow 1$$

2.1 Physical Quantities of Interest

The important physical quantities of interest for the governing flow problem, such as skin friction C_{f_x} , the local Nusselt number Nu_x , and Sherwood number Sh_x are defined as follow.

$$C_{f_x} = \frac{\tau_w}{U_w^2}, \quad Nu_x = \frac{(x+b)q_w}{(T_\infty - T_M)}, \quad Sh_x = \frac{(x+b)j_w}{(C_\infty - C_M)} \quad (25)$$

where $\tau_w = \nu \frac{\partial u}{\partial y}$, $q_w = \frac{\partial T}{\partial y}$ and $j_w = \frac{\partial C}{\partial y}$ at $y = A(x+b)^{\frac{(1-m)}{2}}$, are respectively called the skin friction, the heat flux and the mass flux at the wall. These parameters in dimensionless form can be written as

$$\text{Re}_x^{1/2} C_{f_x} = ((m+1)/2)^{1/2} \left(\frac{\theta_r}{(\theta_r - 1)} \right) f''(0), \quad \text{Re}_x^{-1/2} Nu_x = -((m+1)/2)^{1/2} (1 + \varepsilon_1) \theta'(0) \text{ and}$$

$\text{Re}_x^{-1/2} Sh_x = -((m+1)/2)^{1/2} (1 + \varepsilon_2) \phi'(0)$, where $\text{Re}_x = U_w(x+b)/\nu_\infty$ is called local Reynolds number.

3. Exact Analytical Solutions for Some Special Cases

In this section, we study the exact solutions for some special cases. It is important to analyze some theoretical analysis of the certain solutions for some given physical parameters and these solutions serve as the base function for computing general solutions through numerical schemes. In the case of absence of Casson parameter β , variable fluid viscosity parameter θ_r , stretching rate ratio parameter A^* , and modified Hartman number Q the present problem reduces to Fang et al. [26]. The discussions here will be emphasized on other parameters except $m \neq 1$.

Case (i): when $m = -1/3$ then Eq. (21) reduces to the following form,

$$f''' + ff'' + (f')^2 = 0 \quad (26)$$

with the associated boundary conditions (24) becomes,

$$f(0) = 2\alpha, \quad f'(0) = 1, \quad f'(\infty) = 0 \quad (27)$$

On integration Eq. (26) twice yields to

$$f' + \frac{f^2}{2} = (\gamma + 2\alpha)\eta + (2\alpha^2 + 1) \quad (28)$$

where $\gamma = f''(0)$, in order to have a finite solution it is essential to consider $\gamma = -2\alpha$

$$f' + \frac{f^2}{2} = (2\alpha^2 + 1) \quad \text{when } \xi \rightarrow \infty, \text{ we have } f(\infty) = \sqrt{2 + 4\alpha^2}. \quad (29)$$

The solution is $f(\xi) = \sqrt{2 + 4\alpha^2} \tanh \left[\frac{\sqrt{2 + 4\alpha^2}}{2} \xi + \tanh^{-1} \left(\frac{2\alpha}{\sqrt{2 + 4\alpha^2}} \right) \right]$ and (30)

$$f'(\xi) = 1 + 2\alpha^2 \operatorname{sech}^2 \left[\frac{\sqrt{2 + 4\alpha^2}}{2} \xi + \tanh^{-1} \left(\frac{2\alpha}{\sqrt{2 + 4\alpha^2}} \right) \right] \quad (31)$$

It should be noted that, for $m = -1/3$, the above solutions reduce to the solutions for a flat stretching surface. This confirms that the present numerical solutions are in good agreement with those of Fang *et al.*, [26] and these can be used for numerical code validation in this work.

Case(ii): For $m = -1/2$, we can obtain another analytical solution, for this case, Eq. (21) reduces to,

$$f''' + ff'' + 2(f')^2 = 0 \quad (32)$$

with the respective boundary conditions (24) becomes as,

$$f(0) = 3\alpha, \quad f'(0) = 1, \quad f'(\infty) = 0 \quad (33)$$

Eq. (32) can be written in the form of

$$\frac{1}{f} \frac{d}{d\xi} \left[f^{3/2} \frac{d}{d\xi} \left(f^{-1/2} f' + \frac{2}{3} f^{3/2} \right) \right] = 0 \quad (34)$$

Integrating Eq. (34) once reduces to the following form

$$-\frac{1}{2}(f')^2 + ff'' + f^2 f' = -\frac{1}{2} + 3\alpha\gamma + 9\alpha^2 \quad (35)$$

Applying free boundary condition we get,

$$\gamma = -3\alpha + \frac{1}{6\alpha} \quad (36)$$

On integration Eq. (35) leads to

$$f^{-1/2} f' + \frac{2}{3} f^{3/2} = \frac{2}{3} (3\alpha)^{3/2} + \frac{1}{\sqrt{3\alpha}} \quad (37)$$

The final solution is

$$\xi + D = \frac{1}{2d^2} \ln \left[\frac{f + d\sqrt{f} + d^2}{(d - \sqrt{f})^2} \right] + \frac{\sqrt{3}}{d^2} \tan^{-1} \left(\frac{2\sqrt{f} + d}{d\sqrt{3}} \right) = 0 \quad (38)$$

where

$$d = [(3\alpha)^{3/2} + 3 / (2\sqrt{3\alpha})]^{1/3}$$

and

$$D = \frac{1}{2d^2} \ln \left[\frac{(3\alpha + d\sqrt{3\alpha} + d^2)}{(d - \sqrt{3\alpha})^2} \right] + \frac{\sqrt{3}}{d^2} \tan^{-1} \left(\frac{2\sqrt{3\alpha} + d}{d\sqrt{3}} \right) = 0 \quad (39)$$

Since the system of Eq. (21)-(23) with boundary conditions (24) has no exact analytical solutions, they are solved numerically via a Keller-Box method.

4. Method of Solution

The system of highly nonlinear coupled differential Eq. (21) to (23) along with appropriate boundary conditions in Eq. (24) are solved by finite difference scheme known as Keller Box Method. This system is not conditionally stable and has a second order accuracy with arbitrary spacing. For solving this system first write the differential equations and respective boundary conditions in terms of first order system, which is then, converted into a set of finite difference equations using central difference scheme. Since the equations are highly nonlinear and cannot be solved analytically, therefore these equations are solved numerically using the symbolic software known as Fedora. Further nonlinear equations are linearized by Newton's method and resulting linear system of equations is solved by block tri-diagonal elimination method. For the sake of brevity, the details of the solution process are not presented here. For numerical calculations, a uniform step size is taken which gives satisfactory results and the solutions are obtained with an error tolerance of 10^{-6} in all the cases. To demonstrate the accuracy of the present method, the results for the dimensionless Skin friction, Nussult number and Sherwood number are compared with the previous results.

4.1 Validation of Methodology

The main objective of this section is to check the validation of the present work. The present numerical results are compared with the existing work of Farooq *et al.*, [28] and Prasad *et al.*, [31] in the absence and presence of Riga plate with $Pr = A^* = \varepsilon_1 = \varepsilon_2 = Nt = \lambda = Le = M = 0, Nb \rightarrow 0, \beta \rightarrow \infty, \theta_r \rightarrow \infty$ and the results are in excellent agreement with the previous literature (Table 1).

Table 1

Comparison of Skin friction coefficient $-f''(0)$ for different values of wall thickness parameter α and velocity power index m when the presence and absence of a Riga plate at fixed values of $Pr = A^* = \varepsilon_1 = \varepsilon_2 = Nt = \lambda = Le = M = 0, Nb \rightarrow 0, \beta \rightarrow \infty, \theta_r \rightarrow \infty$.

α	m	Presence of Riga plate Farooq <i>et al.</i> , [28] by OHAM when $Q=0.1, \beta_1=0.2$	Absence of Riga plate Prasad <i>et al.</i> , [31] by OHAM, when $\lambda=0, Mn=Q=\beta_1=0$	Present results, Keller Box Method	
				Presence of Riga plate	Absence of Riga plate
0.25	02	0.9990	1.0614	0.9990	1.06140
	03	1.0465	1.0907	1.0456	1.09050
	05	1.0908	1.1182	1.0902	1.11860
	07	1.1120	1.1328	1.1121	1.13230
	09	1.1244	1.1401	1.1247	1.14041
	10	1.1289	1.1439	1.1288	1.14334
0.5	02	0.9673	1.0231	0.9672	1.02341
	03	0.9976	1.0358	0.9975	1.03588
	05	1.0252	1.0487	1.0253	1.04862
	07	1.0382	1.0551	1.0383	1.05506
	09	1.0458	1.0512	1.0458	1.05893
	10	1.0485	1.0604	1.0485	1.06034

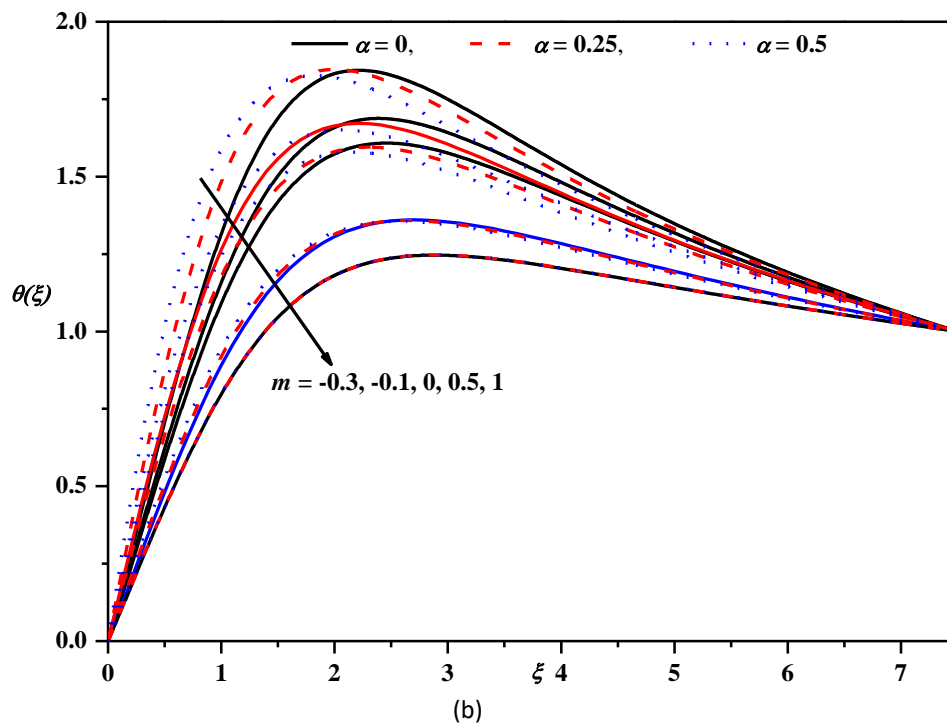
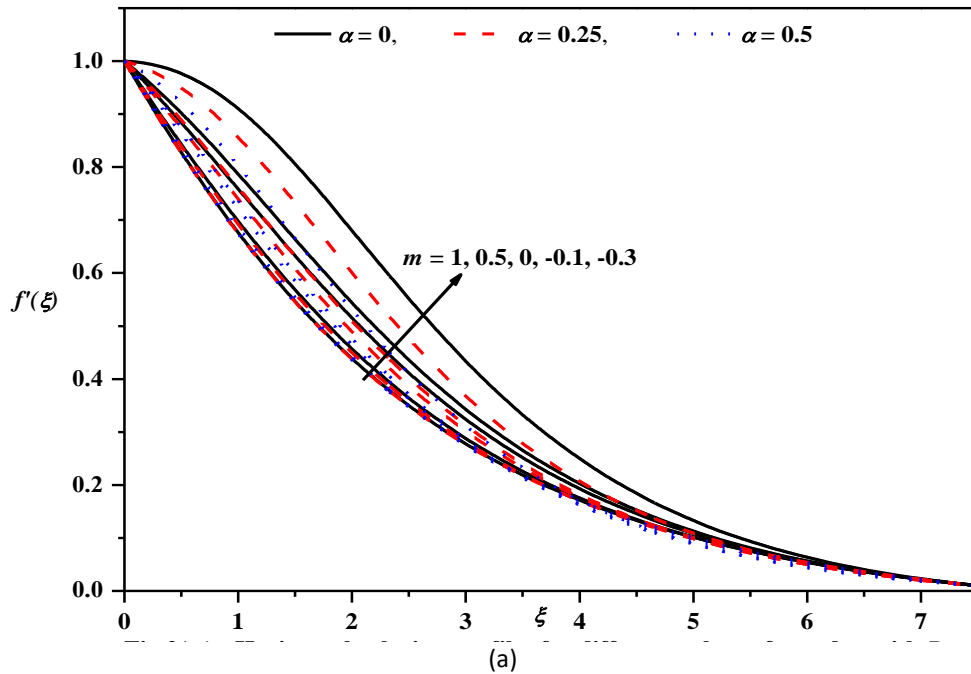
5. Results and Discussion

The system of nonlinear ordinary differential Eq. (21) to (23) together with the appropriate boundary conditions (24) are numerically solved by using Keller Box method. The influence of various physical parameters such as Casson parameter β , variable fluid viscosity parameter θ_r , velocity power index m , stretching rate ratio parameter A^* , modified Hartman number Q , dimensionless parameter β_1 , variable thermal conductivity parameter ε_1 , Brownian motion parameter Nb , thermophoresis parameter Nt , Prandtl number Pr , heat source/sink parameter λ , variable species diffusivity parameter ε_2 , Lewis number Le , and wall thickness parameter α on the horizontal velocity profile $f'(\xi)$, the temperature profile $\theta(\xi)$, and the concentration profile $\phi(\xi)$ are exhibited through Figure 2-9. The computed numerical values for the skin friction $f''(0)$, the Nusselt number $\theta'(0)$ and the wall Sherwood number $\phi'(0)$ are presented in Table 2.

In Table 2 we present the results for $f''(0)$, $\theta'(0)$ and $\phi'(0)$ corresponding to different values of the physical parameters. The skin friction coefficient is a decreasing function of the parameters m , α , β , β_1 , θ_r and increasing function of A^* , Q . Nusselt number reduces for m , α , A^* , ε_1 and increases for β , β_1 , θ_r , Nb , Nt , Pr , and λ . Further, the Sherwood number decreases for β & β_1 and increases for A^* .

The effect of velocity power index m and wall thickness parameter α on velocity, temperature and concentration boundary layers are depicted in Figure 2(a) – 2(c). Figure 2(a) elucidates that, for increasing values of m , $f'(\xi)$ reduce and this is due to the fact that the stretching velocity enhances for larger values of m which causes more deformation in the fluid, consequently velocity profiles decrease. A similar trend may be observed in the case of $\theta(\xi)$ (Figure 2(b)), whereas concentration distribution (Figure 2(c)) shows a dual characteristic, that is for larger values of m concentration profiles reduces near the sheet and opposite behaviour is observed away from the sheet. When $m=1$, the sheet become flat. Similarly, for higher values of wall thickness parameter α , velocity profiles fall, but the temperature distribution upgrade near the sheet and downwards away from the sheet. Whereas, the impact of α is quite opposite in the case of concentration distribution. Figure 3(a) through 3(c) indicates the influence of β and β_1 on $f'(\xi)$, $\theta(\xi)$ and $\phi(\xi)$. For greater values of β velocity profiles are compressed, this is because as β increases the corresponding value of yield stress fall as a result velocity boundary layer thickness decreases. The temperature distribution rises for different estimations of β and concentration distribution exhibits exactly reverse trend. Effect of β_1 on these three profiles is same as that of β . It is noticed from in Figure 4(a) to 4(c) that both θ_r and A^* exhibits opposite trend, increasing variable fluid viscosity reduces the velocity and concentration profiles while the enhancement is observed in the case of temperature profiles. This may be due to the fact that, lesser θ_r implies higher temperature difference between the wall and the ambient nanofluid and the profiles explicitly manifest that θ_r is the indicator of the variation of fluid viscosity with temperature which has a substantial effect on $f'(\xi)$ and hence on $f''(\xi)$, where as in the case of temperature the effect is reversed. Figure 5 illustrates the impact of A^* and Q on $f'(\xi)$. An improvement in A^* corresponds to the enhancement of velocity boundary layer thickness. The enhancement in the velocity profile is observed for amplifying Q . Conventionally the velocity profiles are the decreasing function of Hartman number where as in this case the Lorentz force which is produced due to the magnetic arrays parallel to the surface is responsible for the enhancement of the momentum boundary layer thickness. The influence of Nb and Nt on temperature and concentration distribution are sketched in Figure 6(a) and 6(b). It is seen that the higher values of Nb enhances temperature profiles and its boundary layer thickness, whereas concentration distribution suppressed near the sheet and swells away from the sheet. The larger Nt creates a thermophoresis force which compels the nanoparticles to flow from the hotter region to the colder region which results in raising temperature profiles. In the case of concentration distribution, the dual behavior is noticed which reduces near the sheet and increases away from it (See Figure 6(b)). The characteristic of Prandtl number Pr and variable thermal conductivity parameter ε_1 on temperature distribution is demonstrated in Figure 7. Usually temperature distribution reduces for higher values of Pr and enhances for larger values of ε_1 , but in this work quite opposite behaviour can be seen, this is due to the presence of melting heat transfer parameter M and stretching rate ratio parameter A^* . Figure 8 records the effect of heat source/sink parameter λ on $\theta(\xi)$, an increase in λ means rise in the temperature difference $(T_\infty - T_M)$, which leads to an increment in temperature distribution. Figure 9 is plotted for different values of Le and ε_2 on $\phi(\xi)$. Lower the Brownian diffusion coefficient $D_{B\infty}$ the higher Lewis number: This leads to a decrease in the thickness of the nanoparticle concentration boundary layer. It is interesting to note that a distinct rock bottom in

the nanoparticle volume fraction profiles occur in the fluid adjacent to the boundary for higher values of Le and lower values of ε_2 . This means that the nanoparticle volume fraction near the boundary is lesser than the nanoparticle volume fraction at the boundary; accordingly, nanoparticles are likely to transfer to the boundary.



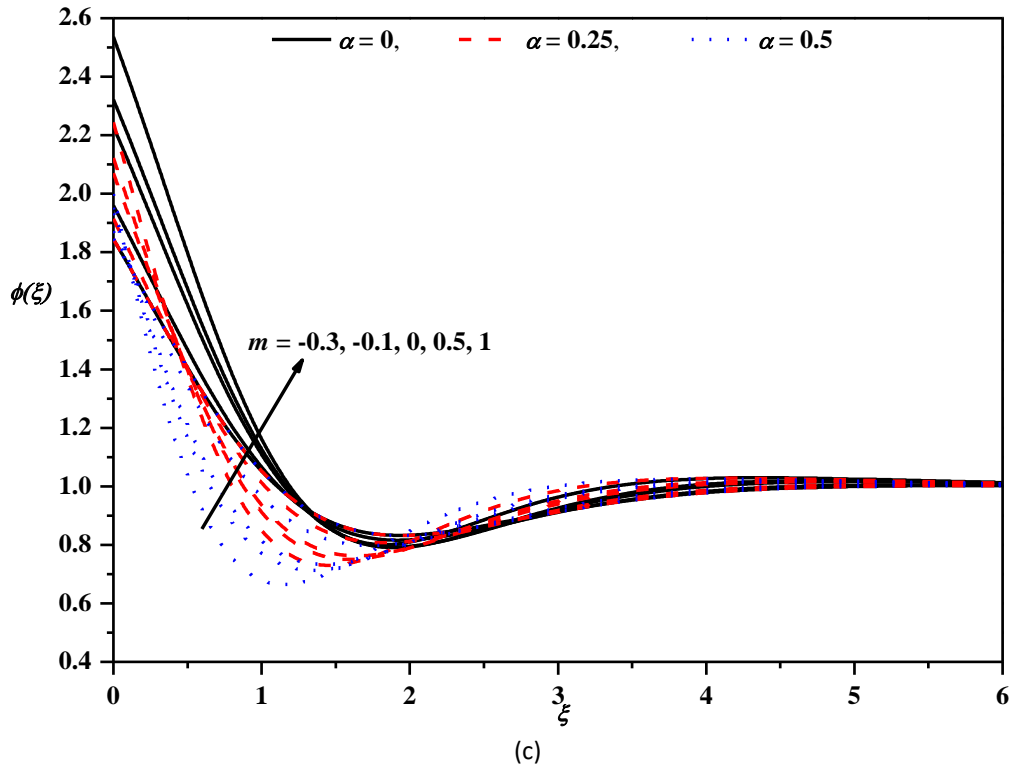
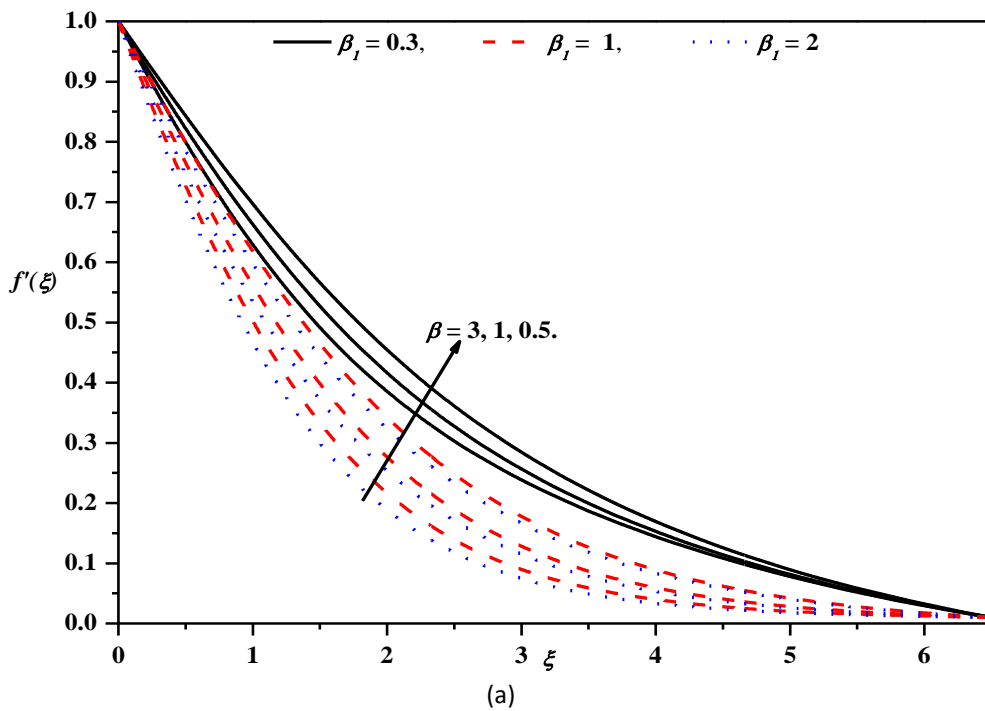


Fig. 2. The effect of velocity power index m and wall thickness parameter α on (a) horizontal velocity, (b) temperature and (c) concentration boundary layers profiles for different values of $Pr = 1$, $Nb = 0.5$, $Nt = 0.5$, $Le = 0.96$, $M = 0.2$, $\lambda = 0.1$, $\varepsilon_1 = 0.1$, $\varepsilon_2 = 0.1$, $\theta_r = -5$, $Q = 0.2$, $\beta_1 = 0.3$, $\beta = 0.2$, $A^* = 0.01$.



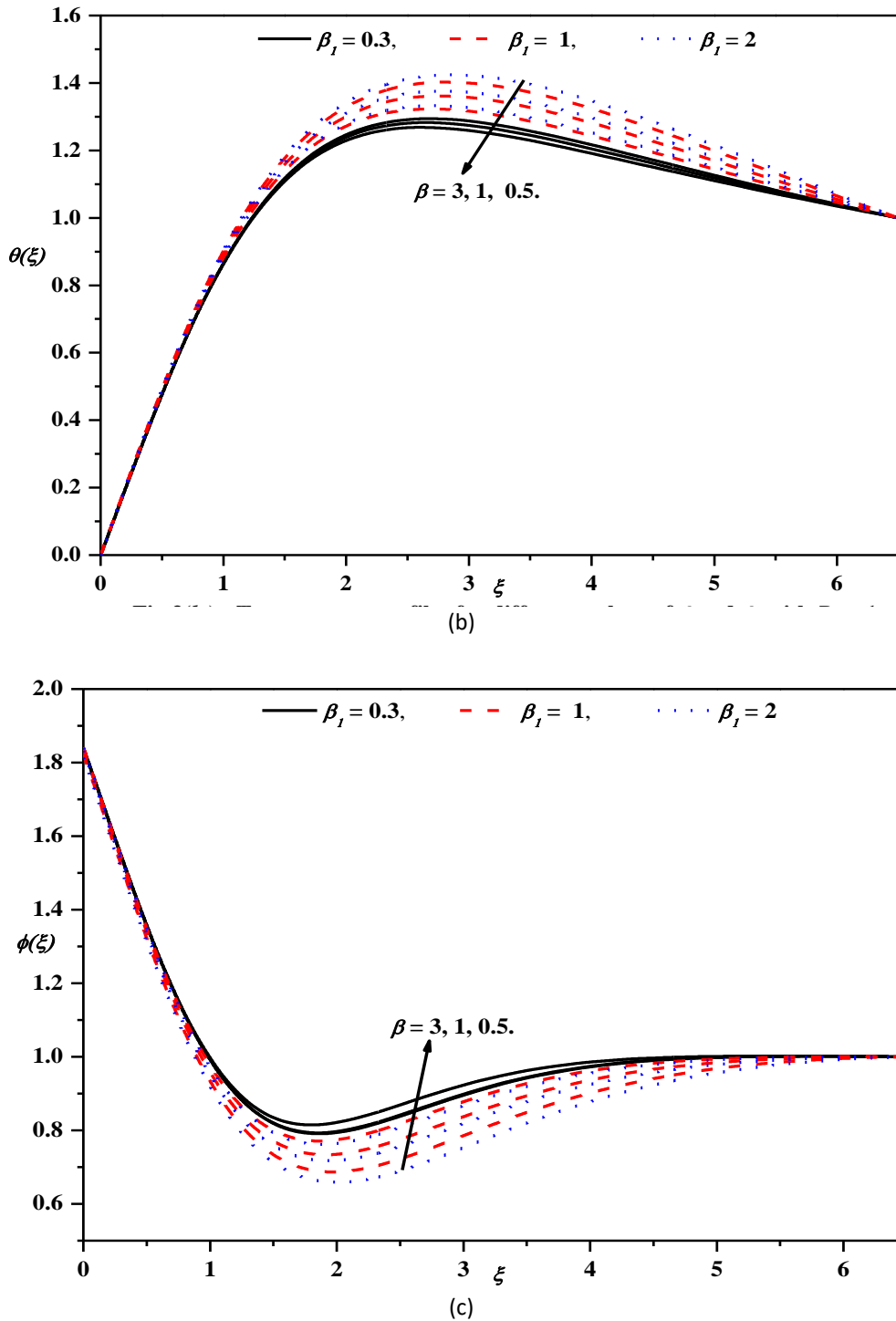
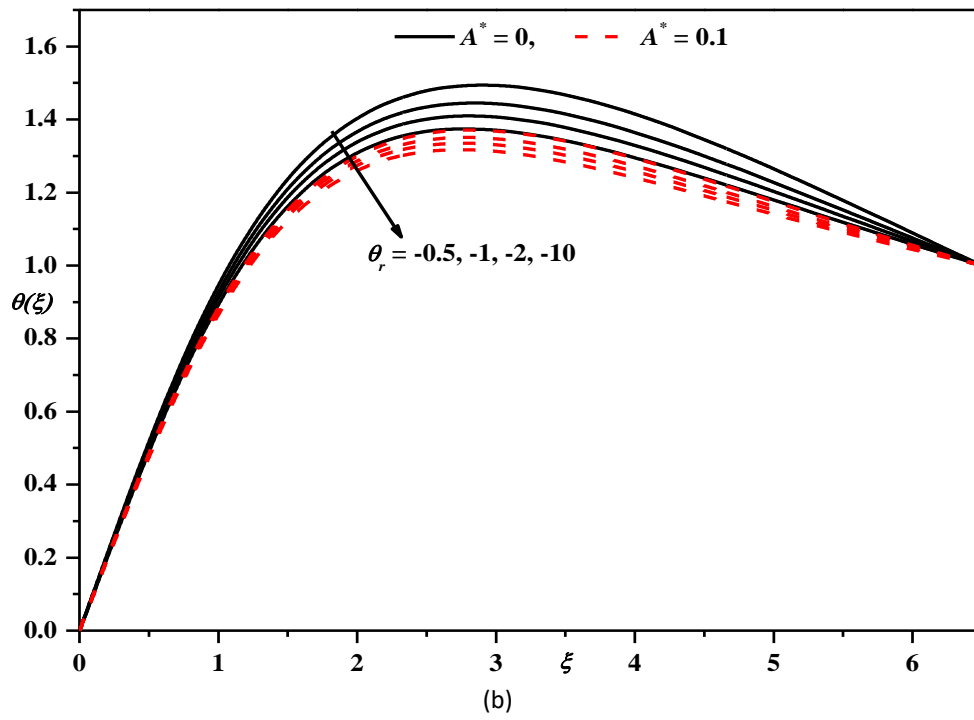
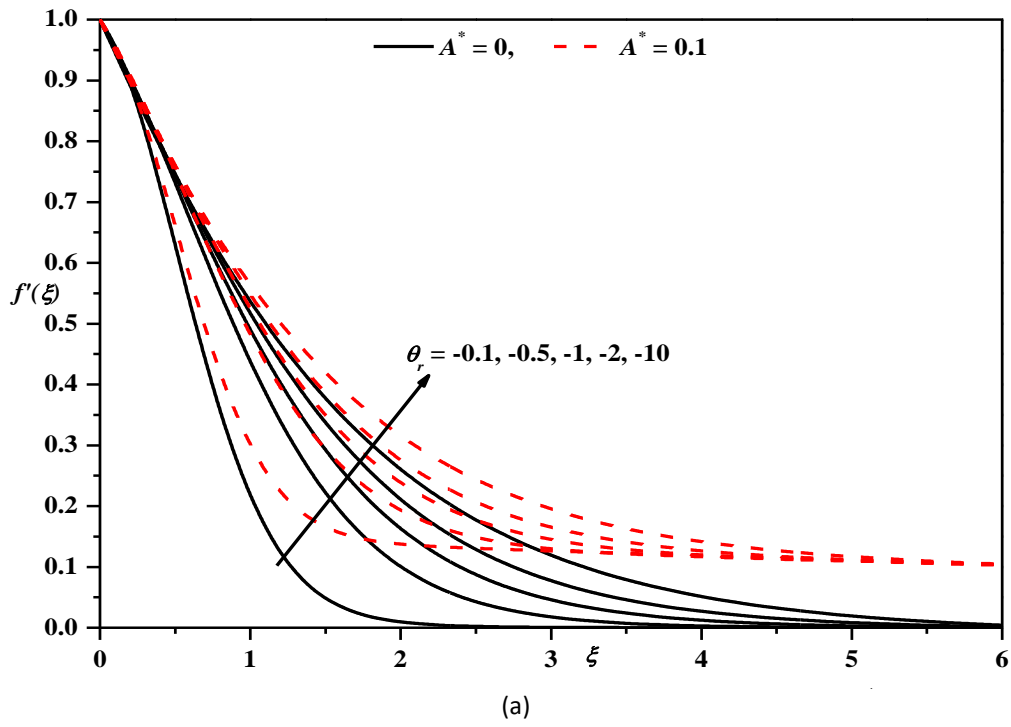


Fig. 3. The influence of β and β_1 on (a) horizontal velocity, (b) temperature and (c) concentration profiles for different values of $Pr = 1$, $Nb = 0.5$, $Nt = 0.5$, $Le = 0.96$, $M = 0.2$, $\lambda = 0.1$, $\varepsilon_1 = 0.1$, $\varepsilon_2 = 0.1$, $\theta_t = -5$, $Q = 0.1$, $\alpha = 0.25$, $A^* = 0.01$



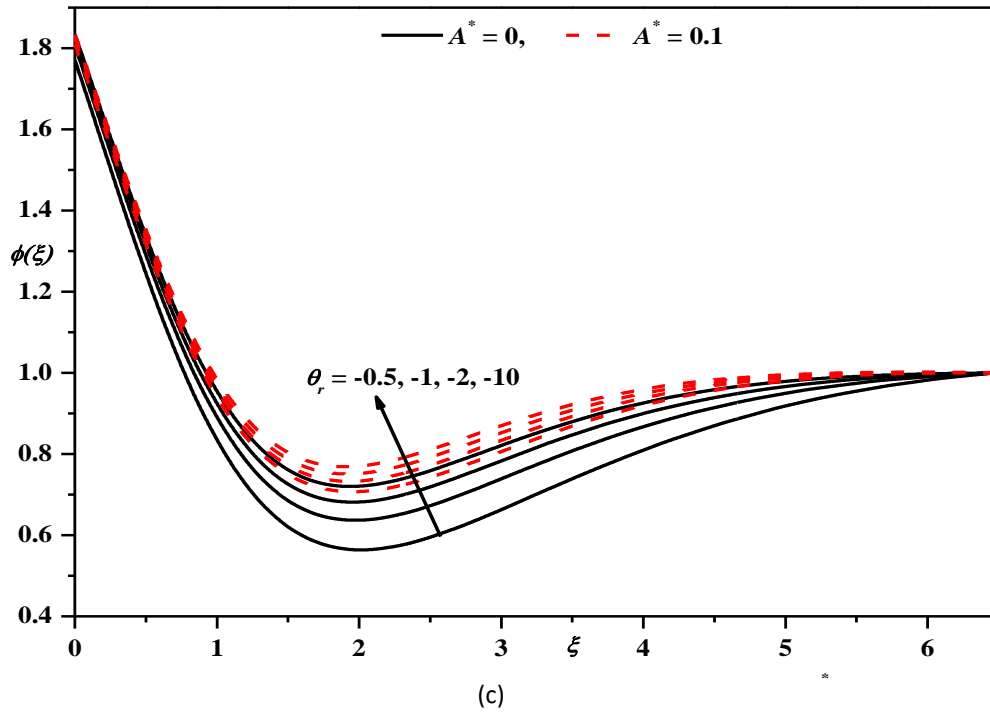


Fig. 4. The (a) horizontal velocity, (b) temperature and (c) concentration profiles for different values of θ_r and A^* with $Pr = 1$, $Nb = 0.5$, $Nt = 0.5$, $Le = 0.96$, $M = 0.2$, $\lambda = 0.1$, $\varepsilon_1 = 0.1$, $\varepsilon_2 = 0.1$, $Q = 1$, $\alpha = 0.25$, $m = 0.5$

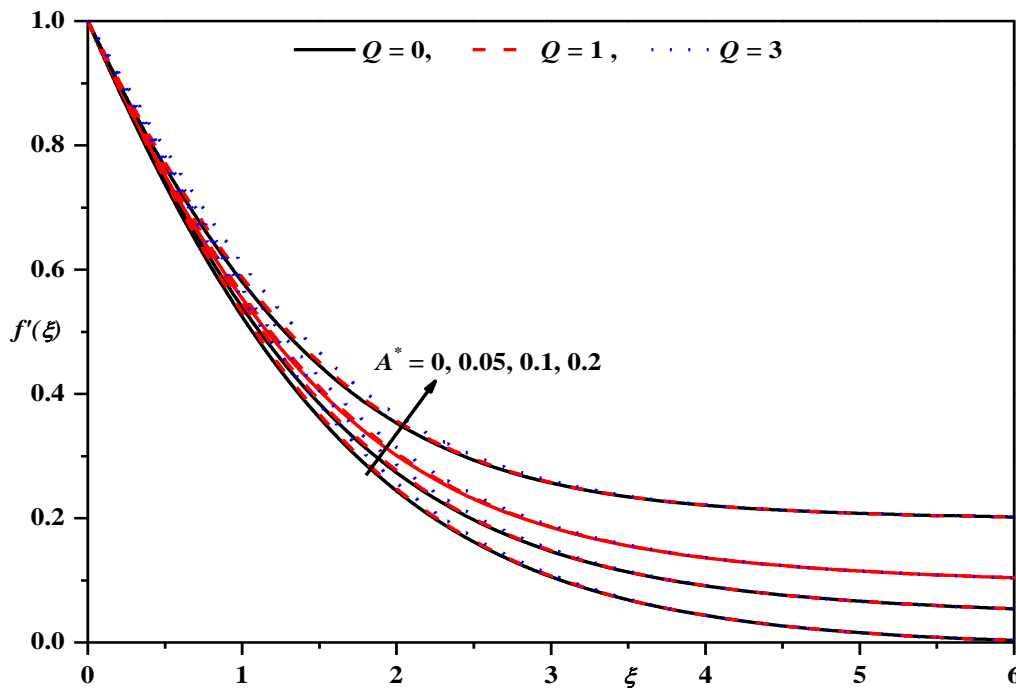


Fig. 5. The horizontal velocity profiles for different values of A^* and Q with $Pr = 1$, $Nb = 0.5$, $Nt = 0.5$, $Le = 0.96$, $M = 0.2$, $\lambda = 0.1$, $\varepsilon_1 = 0.1$, $\varepsilon_2 = 0.1$, $\alpha = 0.25$, $\theta_r = -5$, $m = 0.5$, $\beta_1 = 0.3$ and $\beta = 1$

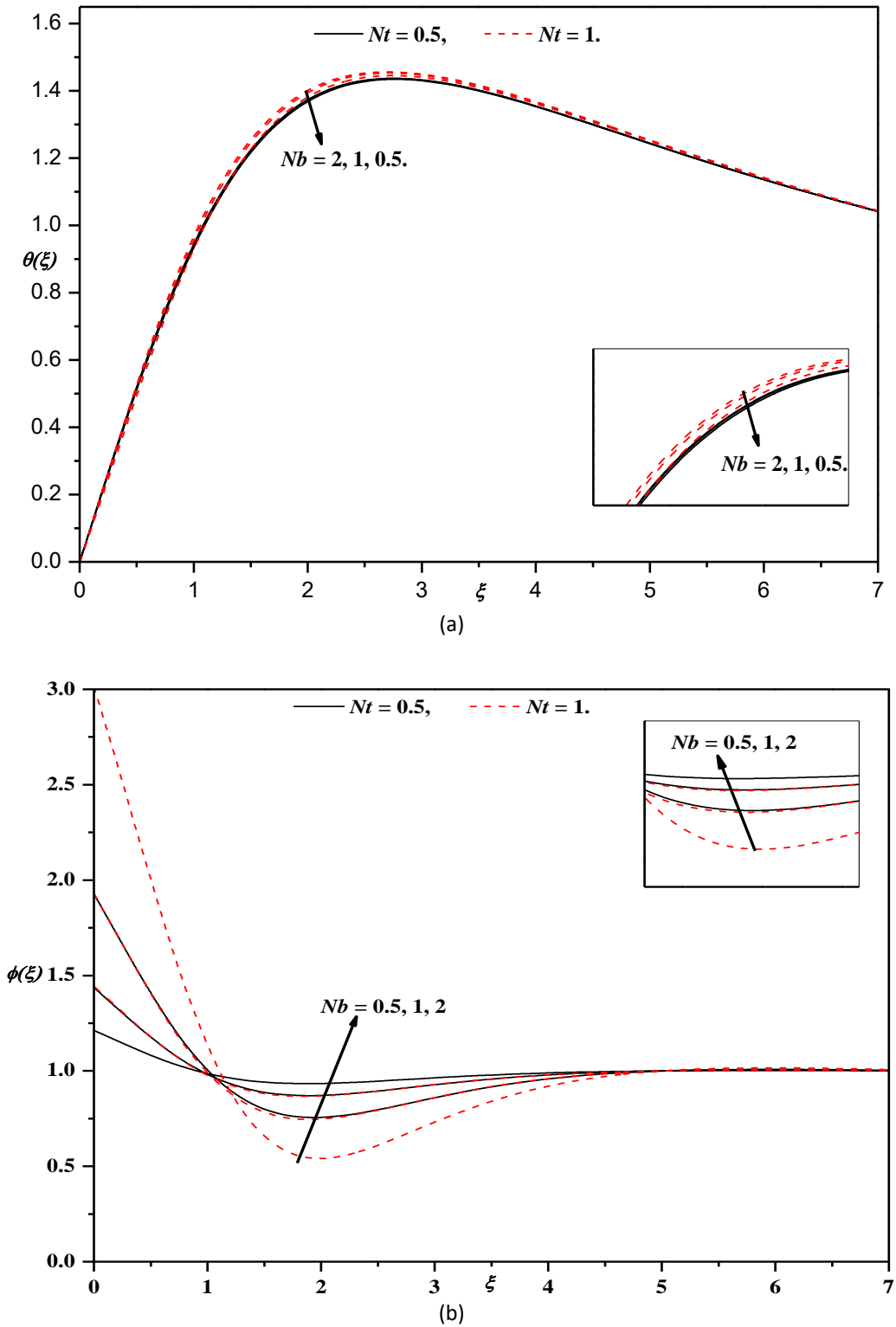


Fig. 6. The influence of Nb and Nt on the (a) temperature and (c) concentration profiles with $Pr = 1$, $Le = 0.96$, $M = 0.2$, $\lambda = 0.1$, $\varepsilon_1 = 0.1$, $\varepsilon_2 = 0.1$, $\alpha = 0.25$, $Q = 1$, $\beta_1 = 2$, $\beta = 1$, $\theta_t = -0.5$ and $A^* = 0.01$

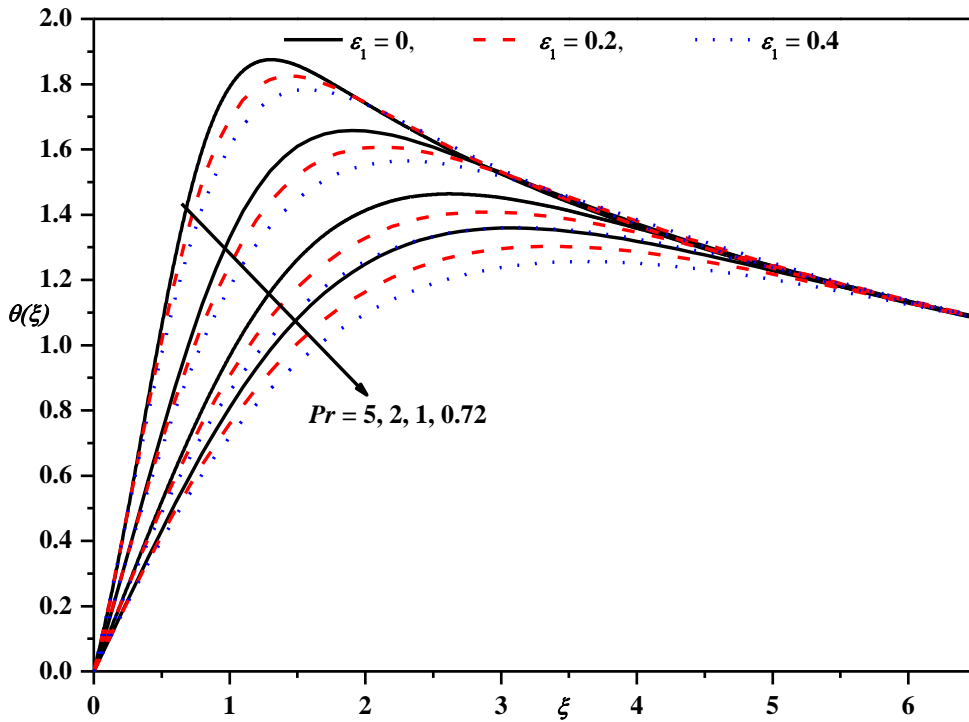


Fig. 7. The temperature profiles for different values of ε_1 and Pr with $m = 0.5$, $Nb = 0.5$, $Nt = 0.5$, $Le = 0.96$, $M = 0.2$, $\lambda = 0.1$, $\varepsilon_2 = 0.1$, $\alpha = 0.25$, $\theta_c = -5$, $Q = 1$, $\beta_1 = 0.3$, $\beta = 1$, and $A^* = 0.01$

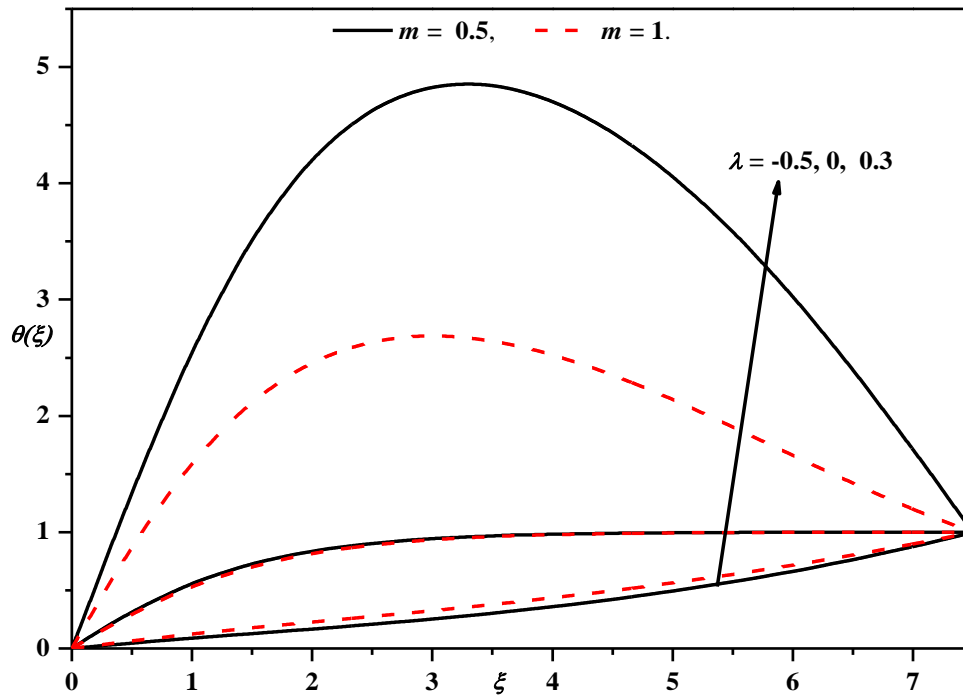


Fig. 8. The temperature profiles for different values of λ and m with $Le = 0.96$, $Nb = 0.5$, $Nt = 0.5$, $M = 0.2$, $\lambda = 0.1$, $\varepsilon_2 = 0.1$, $\alpha = 0.25$, $\theta_c = -5$, $Q = 1$, $\beta_1 = 0.3$, $\beta = 1$, and $A^* = 0.01$

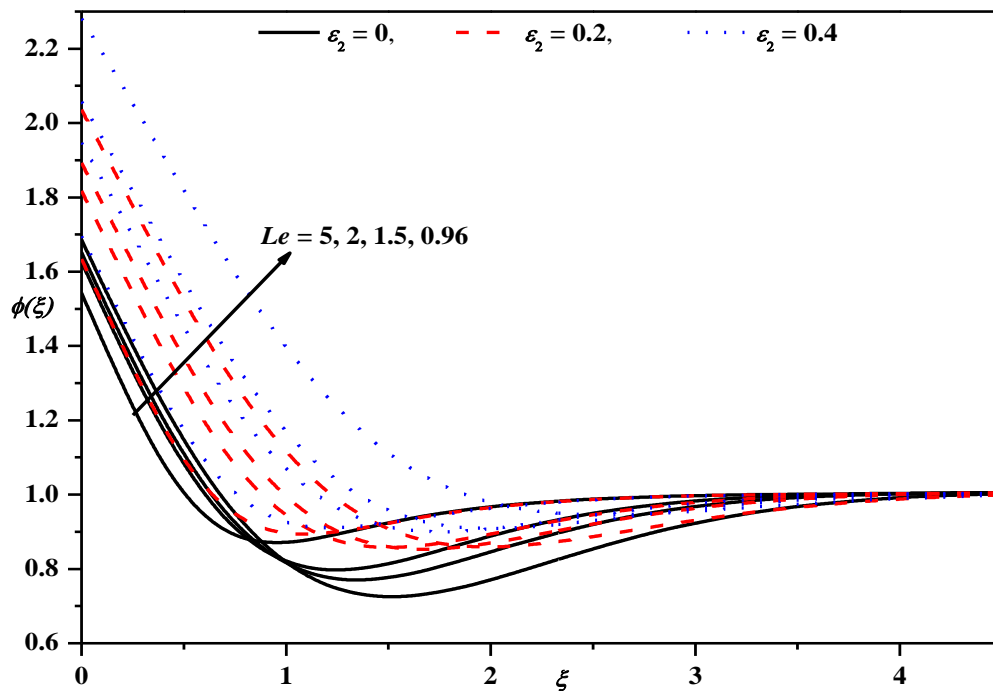


Fig. 9. The concentration profiles for different values of ϵ_2 and Le with $m = 0.5$, $Nb = 0.5$, $Nt = 0.5$, $M = 0.2$, $\lambda = 0.1$, $\alpha = 0.25$, $\theta_t = -5$, $Q = 1$, $\beta_1 = 0.3$, $\beta = 1$, and $A^* = 0.01$

Table 2
 Values of Skin friction, Nusselt number and Sherwood number for different physical parameters

Pr	Le	Nb	Nt	ε_1	ε_2	λ	A*	M	β_1	β	Q	θ_r	m	$\alpha = 0.25$			$\alpha = 0.5$			
														$f''(0)$	$\theta'(0)$	$\phi'(0)$	$f''(0)$	$\theta'(0)$	$\phi'(0)$	
1	0.96	0.5	0.5	0.1	0.1	0.1	0.01	0.2	2	1	0.1	-5	-0.3	-0.0573	1.883	-1.8833	-0.1095	2.4189	-2.4189	
													-0.1	-0.1990	1.520	-1.5201	-0.2243	1.8289	-1.8289	
													0.0	-0.2369	1.390	-1.3905	-0.2561	1.6311	-1.6311	
													0.5	-0.3297	1.025	-1.0256	-0.3356	1.0937	-1.0937	
													1.0	-0.3697	0.8643	-0.8643	-0.3685	0.8643	-0.8643	
Pr	Le	Nb	Nt	ε_1	ε_2	λ	A*	M	m	θ_r	Q	β	α	$\beta_1 = 1.0$			$\beta_1 = 2.0$			
1	0.96	0.5	0.5	0.1	0.1	0.1	0.01	0.2	0.5	-5	0.1	0.25	0.5	-0.4136	0.987	-0.9876	-0.4489	0.9879	-0.9879	
													1.0	-0.4925	0.996	-0.9962	-0.5414	0.9969	-0.9969	
													2.0	-0.5851	1.003	-1.0036	-0.6519	1.0044	-1.0044	
													5.0	-0.6114	1.004	-1.0045	-0.6839	1.0056	-1.0056	
Pr	Le	Nb	Nt	ε_1	ε_2	λ	A*	M	β_1	Q	θ_r	β	α	$m = 0.5$			$m = 1.0$			
1	0.96	0.5	0.5	0.1	0.1	0.1	0.1	0.2	2	1	-2.0	1	0.25	-10	-0.5288	0.968	-0.9682	-0.5628	0.8093	-0.8093
														-5.0	-0.5165	0.971	-0.9710	-0.5516	0.8105	-0.8105
														-2.0	-0.4863	0.977	-0.9776	-0.5234	0.8128	-0.8128
														-1.0	-0.4494	0.984	-0.9842	-0.4878	0.8143	-0.8143
														-0.5	-0.4009	0.989	-0.9890	-0.4395	0.8152	-0.8152
θ_r	Le	Nb	Nt	A*	ε_2	λ	m	M	β_1	Pr	Q	β	α	$\varepsilon_1 = 0.2$			$\varepsilon_1 = 0.4$			
-5	0.96	0.5	0.5	0.01	0.1	0.1	0.5	0.2	2	1.0	0.1	1	0.25	0.72	-0.5275	0.873	-0.8735	-0.5283	0.8758	-0.8758
														1.0	-0.5113	1.042	-1.0429	-0.5118	1.0531	-1.0531
														2.0	-0.4932	1.394	-1.3949	-0.4934	1.4314	-1.4314
														5.0	-0.4844	1.681	-1.6814	-0.4850	1.7462	-1.7462
Pr	Le	m	λ	A*	ε_2	β_1	ε_1	M	Nb	θ_r	Q	β	α	$Nt = 0.5$			$Nt = 1$			
1.0	0.96	0.5	0.1	0.01	0.1	0.3	0.1	0.2	1.0	-5	0.1	1	0.25	0.5	-0.5111	1.036	-1.0366	-0.5149	0.9594	-1.9188
														1.0	-0.5101	1.054	-1.5272	-0.5113	1.0229	-1.0229
														2.0	-0.3415	4.900	-3.6755	-0.5096	1.0544	-0.5272
β_1	M	Nb	Nt	A*	ε_1	m	λ	Le	Pr	θ_r	Q	β	α	$\varepsilon_2 = 0.2$			$\varepsilon_2 = 0.2$			
0.3	0.2	0.5	0.5	0.01	0.1	0.5	0.1	1.5	-0.3365	1.0526	-1.0526	-0.3394	0.9289	-0.9289						
								2.0	-0.3358	1.0755	-1.0755	-0.3385	0.9599	-0.9599						
								5.0	-0.3339	1.1495	-1.1495	-0.3359	1.0579	-1.0579						

6. Conclusions

The present article examines the effects of variable fluid properties on the heat transfer characteristics of a Casson nanofluid over a slender Riga plate with zero mass flux and melting heat transfer boundary conditions. Here, the thickness of the sheet is erratic. The critical points of the present study are summarized as follows:

- i. The effect of velocity power index m on velocity and temperature field is similar, that is, in both the cases the profiles increases as m reduces, whereas in the case of concentration distribution dual nature is observed.
- ii. Velocity and concentration distributions reduces for increasing values of Casson parameter, but the temperature distributions show exactly opposite behavior for larger values of Casson parameter.
- iii. Enhanced variable fluid viscosity parameter influences the velocity and temperature field in opposite manner.
- iv. The modified Hartmann number enhances the velocity distribution and reduces the temperature distribution.
- v. The squeezed thermal boundary layer is observed for the increasing values of variable thermal conductivity parameter.
- vi. The concentration distribution improves for higher values of variable species diffusivity parameter. The dual nature of the concentration profiles is recorded for the Brownian motion parameter and thermophoresis parameter.

Acknowledgement

This research was funded by a grant from Government of India, Ministry of Tribal Affairs (Scholarship Division), New Delhi for supporting financially under Scheme of National Fellowship and Scholarship for Higher Education. (Grant No. 2017-18-NFST-KAR-00764).

References

- [1] Gailitis, A. and Lielausis, O. "On a possibility to reduce the hydrodynamic resistance of a plate in an electrolyte." *Appl. Magnetohydrodynamics Rep.Inst. Phys. Inst. Riga* 13, (1961): 143-146.
- [2] Grinberg, E. "On determination of properties of some potential fields." *Applied Magnetohydrodynamics* 12, (1961): 147-154.
- [3] Tsinober, A. B., and A. G. Shtern. "Possibility of increasing the flow stability in a boundary layer by means of crossed electric and magnetic fields." *Magnetohydrodynamics* 3, no. 2 (1967): 152-154.
- [4] Pantokratoras, Asterios, and Eugen Magyari. "EMHD free-convection boundary-layer flow from a Riga-plate." *Journal of Engineering Mathematics* 64, no. 3 (2009): 303-315.
- [5] Pantokratoras, Asterios. "The Blasius and Sakiadis flow along a Riga-plate." *Progress in Computational Fluid Dynamics, An International Journal* 11, no. 5 (2011): 329-333.
- [6] Choi, Stephen US, and Jeffrey A. Eastman. *Enhancing thermal conductivity of fluids with nanoparticles*. No. ANL/MSD/CP-84938; CONF-951135-29. Argonne National Lab., IL (United States), 1995.
- [7] Buongiorno, Jacopo. "Convective transport in nanofluids." *Journal of Heat Transfer* 128, no. 3 (2006): 240-250.
- [8] Makinde, Oluwole D., and A. Aziz. "Boundary layer flow of a nanofluid past a stretching sheet with a convective boundary condition." *International Journal of Thermal Sciences* 50, no. 7 (2011): 1326-1332.
- [9] Ahmad, Adeel, Saleem Asghar, and Sumaira Afzal. "Flow of nanofluid past a Riga plate." *Journal of Magnetism and Magnetic materials* 402 (2016): 44-48.
- [10] Ayub, M., T. Abbas, and M. M. Bhatti. "Inspiration of slip effects on electromagnetohydrodynamics (EMHD) nanofluid flow through a horizontal Riga plate." *The European Physical Journal Plus* 131, no. 6 (2016): 193.
- [11] Hayat, T., Mumtaz Khan, M. Imtiaz, and A. Alsaedi. "Squeezing flow past a Riga plate with chemical reaction and convective conditions." *Journal of Molecular Liquids* 225 (2017): 569-576.

- [12] Hayat, Tasawar, Mumtaz Khan, Muhammad Ijaz Khan, Ahmed Alsaedi, and Muhammad Ayub. "Electromagneto squeezing rotational flow of Carbon (C)-Water (H₂O) kerosene oil nanofluid past a Riga plate: A numerical study." *PloS one* 12, no. 8 (2017): e0180976.
- [13] Naveed, A., Fitnat, S., Umar, K., Ilyas, K., Tawfeeq, A. A., Imran, F. and Syed, T. Mohyud-Din. "Spherical shaped (Ag-Fe₃O₄/H₂O) hybrid nanofluid flow squeezed between two Riga plates with nonlinear thermal radiation and chemical reaction effects." *Energies* 12, no. 1 (2019): 76.
- [14] Sheikholeslami, Mohsen, and Houman B. Rokni. "Effect of melting heat transfer on nanofluid flow in existence of magnetic field considering Buongiorno Model." *Chinese Journal of Physics* 55, no. 4 (2017): 1115-1126.
- [15] Wakif, Abderrahim, Zoubair Boulahia, Farhad Ali, Mohamed R. Eid, and Rachid Sehaqui. "Numerical analysis of the unsteady natural convection MHD couette nanofluid flow in the presence of thermal radiation using single and two-phase nanofluid models for Cu-Water nanofluids." *International Journal of Applied and Computational Mathematics* 4, no. 3 (2018): 81.
- [16] Wakif, Abderrahim, Zoubair Boulahia, and Rachid Sehaqui. "A semi-analytical analysis of electro-thermo-hydrodynamic stability in dielectric nanofluids using Buongiorno's mathematical model together with more realistic boundary conditions." *Results in Physics* 9 (2018): 1438-1454.
- [17] Wakif, Abderrahim, Zoubair Boulahia, S. R. Mishra, Mohammad Mehdi Rashidi, and Rachid Sehaqui. "Influence of a uniform transverse magnetic field on the thermo-hydrodynamic stability in water-based nanofluids with metallic nanoparticles using the generalized Buongiorno's mathematical model." *The European Physical Journal Plus* 133, no. 5 (2018): 181.
- [18] Reza, Jawad, Fateh Mebarek-Oudina, and Oluwole Daniel Makinde. "MHD slip flow of Cu-Kerosene nanofluid in a channel with stretching walls using 3-stage Lobatto IIIA formula." In *Defect and Diffusion Forum*, vol. 387, pp. 51-62. Trans Tech Publications, 2018.
- [19] Prasad, K. V., Hanumesh Vaidya, Oluwole Daniel Makinde, and B. Srikantha Setty. "MHD mixed convective flow of Casson nanofluid over a slender rotating disk with source/sink and partial slip effects." In *Defect and Diffusion Forum*, vol. 392, pp. 92-122. Trans Tech Publications, 2019.
- [20] Mebarek-Oudina, Fateh. "Convective heat transfer of Titania nanofluids of different base fluids in cylindrical annulus with discrete heat source." *Heat Transfer—Asian Research* 48, no. 1 (2019): 135-147.
- [21] Hayat, Tasawar, Taseer Muhammad, Sabir Ali Shehzad, and Ahmed Alsaedi. "An analytical solution for magnetohydrodynamic Oldroyd-B nanofluid flow induced by a stretching sheet with heat generation/absorption." *International Journal of Thermal Sciences* 111 (2017): 274-288.
- [22] Daniel, Yahaya Shagaiya, Zainal Abdul Aziz, Zuhaila Ismail, and Faisal Salah. "Impact of thermal radiation on electrical MHD flow of nanofluid over nonlinear stretching sheet with variable thickness." *Alexandria Engineering Journal* 57, no. 3 (2018): 2187-2197.
- [23] Hayat, Tasawar, Madiha Rashid, Ahmed Alsaedi, and Bashir Ahmad. "Flow of nanofluid by nonlinear stretching velocity." *Results in Physics* 8 (2018): 1104-1109.
- [24] El-Aziz, M. Abd, and A. A. Afify. "Effect of Hall current on MHD slip flow of Casson nanofluid over a stretching sheet with zero nanoparticle mass flux." *Thermophysics and Aeromechanics* 26, no. 3 (2019): 429-443.
- [25] Rajashekhar, C., G. Manjunatha, Hanumesh Vaidya, B. Divya, and K. Prasad. "Peristaltic flow of Casson liquid in an inclined porous tube with convective boundary conditions and variable liquid properties." *Frontiers in Heat and Mass Transfer (FHMT)* 11 (2018).
- [26] Fang, T., Zhang, J. and Zhong. Y. "Boundary layer flow over a stretching sheet with variable thickness." *Applied Mathematics and Computations* 218, (2012): 7241-7252.
- [27] Khader, M. M. and Megahed, A. M. "Boundary layer flow due to a stretching sheet with a variable thickness and slip velocity." *Journal of Applied Mechanics and Technical Physics* 56, (2015): 241-247.
- [28] Farooq, M., Anjum, A., Hayat, T. and Alsaedi, A. "Melting heat transfer in the flow over a variable thicked Riga plate with homogeneous-heterogeneous reactions." *Journal of Molecular liquids* 224, (2016): 1341-1347.
- [29] Prasad, K. V., Hanumesh, V., Vajravelu. K. and Rashidi, M. M. "Effects of variable fluid properties on MHD flow and heat transfer over a stretching sheet with variable thickness." *Journal of Mechanics* 33, (2016): 501-512.
- [30] Prasad, K. V., Vajravelu, K., Hanumesh, V. and Robert A. Van Gorder. "MHD flow and heat transfer in a nanofluid over a slender elastic sheet with variable thickness." *Results in Physics* 7, (2017): 1462-1474.
- [31] Prasad, K. V., Hanumesh, V., Vajravelu, K. and Ramanjini, V. "Analytical study of Cattaneo-Christov heat flux model for Williamson -Nanofluid flow over a slender elastic sheet with variable thickness." *Journal of Nanofluids* 7, (2018): 583-594.

-
- [32] Prasad, K.V., Hanumesh V., Vajravelu, K., Neelufer. Z. Basha and Umesh, V. "Thermal and species concentration of MHD Casson fluid at a vertical sheet in the presence of variable fluid properties." *Ain Shams Engineering Journal* 9, no. 4 (2018): 1763-1779.
- [33] Prasad, K., Hanumesh Vaidya, K. Vajravelu, and U. Vishwanatha. "Influence of Variable Liquid Properties on Mixed Convective MHD Flow over a Slippery Slender Elastic Sheet with Convective Boundary Condition." *Journal of Advanced Research in Fluid Mechanics and Thermal Sciences* 56, no. 1 (2019): 100-123.
- [34] Vajravelu, Kuppapalle, and Kerehalli V. Prasad. *Keller-box method and its application*. Vol. 8. Walter de Gruyter GmbH & Co KG, 2014.